An EV Integrated Isolated DC Charger using a Six-Phase Synchronous Machine

Sukhjit S Ghumman, Mehanathan Pathmanathan, Peter W Lehn
Department of Electrical and Computer Engineering, University of Toronto
Toronto, Ontario, Canada
E-Mail: sukhjit.singh@mail.utoronto.ca
meha.pathmanathan@utoronto.ca
lehn@ece.utoronto.ca

Acknowledgements

This work was supported by the Natural Sciences and Engineering Research Council of Canada (NSERC) under Grant CRDPJ 513206-17.

Keywords

«Electric Vehicles», «DC Chargers», «Onboard Chargers», «Isolated Charging», «Integrated Charger» «Six-Phase Machine» «Multiphase Machine» «WFSM» «WRSM» «PMSM».

Abstract

This paper presents an integrated DC charger using a six-phase synchronous machine with two isolated neutrals. The synchronous motor provides isolation between the DC grid and the battery and does not require a separate transformer. Control techniques are developed which allow charging without generating electromechanical torque inside the machine. The concept is validated experimentally using a six-phase, wound field synchronous machine (WFSM), showing isolated DC charging with zero torque production. Simulation results using an equivalent permanent magnet synchronous machine (PMSM) model are provided, indicating the potential for this system as a means to achieve high-power, high-efficiency isolated DC charging.

Introduction

Multiphase machines have been explored in literature for high-power electromechanical energy conversion applications like wind turbines, electric ships, aerospace, etc. Specifically, six and nine-phase induction and synchronous machines have been studied, as off-the-shelf three-phase converters can be used. Multi-phase machines allow the splitting of current into more paths hence, multiple smaller power electronic converters (modular design), lower torque ripple compared to their three-phase counterparts, increased degrees of freedom, and can facilitate fault-tolerant operations [1]. Due to the aforementioned benefits, multiphase synchronous, induction, and switched reluctance machines have been considered in electric vehicles (EVs) for driving purposes. Recently, multiphase machines have found an interest in EV charging also, as the machine leakage inductances can be used as a filter during the power transfer [2]. In addition, these machines can integrate dissimilar energy sources like fuel cells, supercapacitors etc. [3].

Electric vehicle chargers can be broadly categorized into integrated and non-integrated variants. Non-integrated chargers (which can be off-board fast-charging stations or onboard chargers) usually include a galvanic isolation stage either at line frequency or through an isolated DC/DC converter. In contrast, integrated chargers usually do not provide the means for galvanic isolation [4]. The lack of a galvanic isolation stage (and the inherent large common-mode impedance it provides) can make it challenging for integrated chargers to meet the common-mode leakage current requirements from standards such as UL2231 and IEC61851 (though non-isolated standard-compliant integrated solutions are possible [5]).

Three different charging types exist, namely: 1-ϕ ac, 3-ϕ ac, and DC charging. Various integrated topologies using multi-phase machines have been published [2], but these topologies lack isolation between the input source and the battery unless additional transformers are used. A few solutions have been found in the literature, which allow isolation using multiphase machines. A 3-ϕ wound-field induction machine has been used in [6] for 3-ϕ charging, where the rotor acts as an input port and provides isolation. However, the torque is generated during charging and this method requires mechanical brakes to block the rotor during the charging process. A 3-ϕ ac charger based on a split winding 3-ϕ phase permanent magnet machine is presented in [7] but requires switches to split motor windings during driving and charging operation. Again, this method results in torque production. Therefore, a clutch is needed to decouple the traction motor from the EV powertrain during charging. [8] shows another 3-ϕ charger using a six-phase induction machine as a transformer, but uses switches in the rotor circuit to disconnect it during charging operation. Another topology has been published in [9] for a three-phase grid charging solution that provides isolation, where 1-ϕ ac and 3-ϕ ac grid charging is achieved using a six-phase PMSM. This topology requires additional grid-connected inductors and a three-phase diode bridge on the battery side during the charging process. Therefore, requires additional components and reconfigurations to charge the battery and provide isolation.

To date, DC charging solutions using multi-phase machines, especially integrated DC charging solutions with isolation have not yet been explored. Most EVs use synchronous machines (SM) as they provide high torque density compared to induction machines (IM). In synchronous machines, permanent magnet synchronous machines (PMSM) are more prevalent than wound field synchronous machines (WFSM) due to higher torque density and no additional hardware requirement for the field circuit [10]. This paper investigates machine-integrated DC charging solutions while using the synchronous machine as a medium of isolation. The proposed charger topology and control algorithm are validated experimentally using a six-phase WFSM, showing that isolated DC charging with zero torque production is achieved. Finally, simulation results with an equivalent PMSM model are shown indicating the improvements in efficiency and charging power that can be obtained with an equivalent six-phase PMSM.

Charger Topology

The proposed charger, shown in Fig. 1, uses two three-phase voltage source converters (converter1 and converter2) and a six-phase synchronous machine with two isolated three-phase windings (Y-configuration). Isolated neutrals of Y-connected three-phase windings have been leveraged to provide galvanic isolation between the DC grid and the battery. A two-pole contactor with (S_{1+} & S_{1-}) is the additional component required for reconfiguring the system between charging and driving operation. S_{1+} & S_{1-} remain closed during driving and open during charging operation and the DC-link of converter1 is used as an inlet from the DC grid.

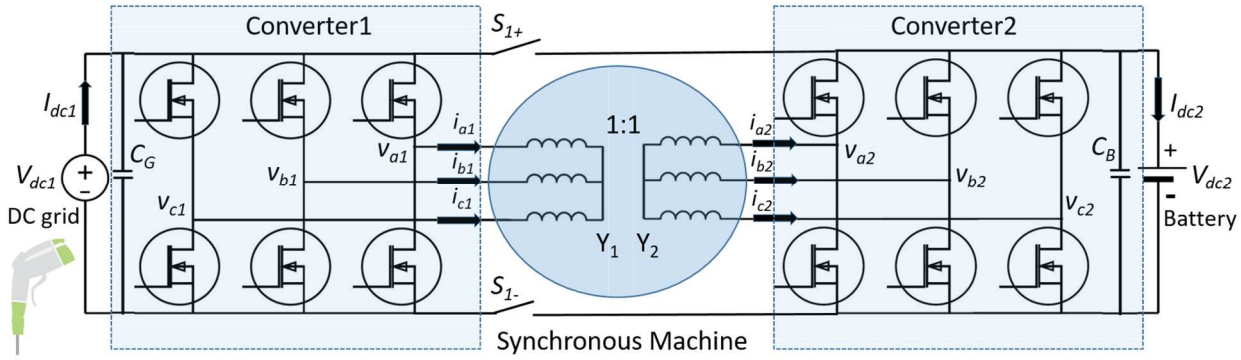

Fig 1: Integrated DC charger using a six-phase synchronous machine as a medium of isolation

The power injected from the DC grid goes through the converter1, which converts it to ac power and transfers it to the winding set2 magnetically, where converter2 converts it back to DC to charge the battery. If suitably oriented, the magnetic field created by stator windings does not introduce torque in the machine, as the torque-producing component does not get excited. The rotor field winding should be kept short-circuited during the charging process, as the proposed control algorithm will result in large voltages being induced across the field winding if it is left open-circuited. The charger has bidirectional power transfer capability, where it can be used for vehicle to vehicle charging (V2V), vehicle to grid (V2G) & V2X (for DC power) capability as well, although, this paper will only focus on DC grid to battery charging.

Machine modeling

The machine used for the proposed charger topology is a six-phase wound field synchronous machine (WFSM) with two isolated neutrals. The two-stator windings have a 0° phase shift between them, Fig 2(a). A Six-phase synchronous machine model using the double dq model ($d_1q_1 0_1$, $d_2q_2 0_2$) in the rotor reference frame is shown in Fig 2(b) and (c) for the charging mode [11], [12]. Zero sequence components will not be discussed here, as there will not be any path for them to flow due to the wye-connected windings. Machine stator voltage equations in the dq axes can be given by (1) – (4), where λ is flux linkage, ω_r is the rotor speed in electrical radians per second (zero, during charging), and p is the time derivative. The stator flux linkage equations are given in (4) - (8) where l_{ls1} and l_{ls2} are the stator leakage inductances, l_{md} and l_{mq} is the d and q-axis magnetizing inductances. As discussed in the previous section, the field winding circuit is short-circuited to avoid high voltages being induced.

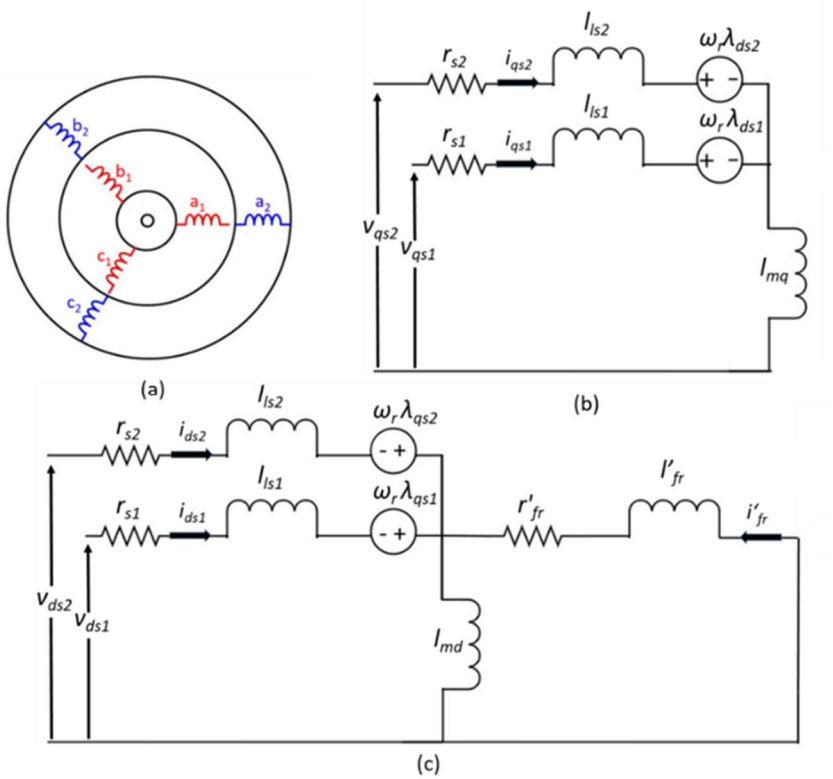

Fig. 2: (a) Six-phase synchronous machine with 0° phase shift between two sets of windings (rotor standstill) (b) q-axis (c) d-axis equivalent circuit referred to the winding set1

$$v_{ds1} = r_{s1} i_{ds1} + p\lambda_{ds1} - \omega_r \lambda_{qs1} \quad (1)$$

$$v_{ds2} = r_{s1} i_{ds2} + p\lambda_{ds2} - \omega_r \lambda_{qs2} \quad (2)$$

$$v_{qs1} = r_{s1} i_{qs1} + p\lambda_{qs1} + \omega_r \lambda_{ds1} \quad (3)$$

$$v_{qs2} = r_{s1} i_{qs2} + p\lambda_{qs2} + \omega_r \lambda_{ds2} \quad (4)$$

$$\lambda_{ds1} = l_{ls1} i_{ds1} + l_{md}(i_{ds1} + i_{ds2} + i'_{fr}) \quad (5)$$

$$\lambda_{ds2} = l_{ls2} i_{ds2} + l_{md}(i_{ds1} + i_{ds2} + i'_{fr}) \quad (6)$$

$$\lambda_{qs1} = l_{ls1} i_{qs1} + l_{mq}(i_{qs1} + i_{qs2}) \quad (7)$$

$$\lambda_{qs2} = l_{ls2} i_{qs2} + l_{mq}(i_{qs1} + i_{qs2}) \quad (8)$$

Charging Operation

The charging algorithm should ensure zero torque production and allow power to be transferred magnetically between two sets of three-phase windings. The following subsections explain the zero torque production, power flow, and control mechanisms during the charging operation.

Zero torque production

Equation (9) gives the electromagnetic torque developed by the machine in a rotor reference frame using the double *dq* model, where *P* represents the number of pole pairs. The rotor is assumed to be at standstill. Zero torque can be achieved if the stator currents of the q-axis are both set to zero.

$$T = \frac{3}{2} P\left[(i_{qs1} + i_{qs2}) l_{md}(i_{ds1} + i_{ds2} + i'_{fr}) - (i_{ds1} + i_{ds2} + i'_{fr}) l_{mq}(i_{qs1} + i_{qs2})\right] \quad (9)$$

Sinusoidal time-varying d-axes currents

The desired ac power can be transferred between the two sets of windings magnetically if time-varying d-axes currents are used. The time-varying d-axes currents in rotor reference will produce a pulsating magnetic field that does not rotate in space and accordingly does not produce electromagnetic torque. This pulsating magnetic field generated by the injection of a time-varying d-axis current in one set of windings will however induce voltages on the second set of windings (and also the field winding, which is why the field must be shorted during this process). The induced voltage on the second set of windings can be leveraged as a means to achieve isolated power transfer from one stator winding set to another. Fig. 3 shows the sample currents in winding set1 and set2 that generate no torque and only d-axis current can be allowed, therefore, the distribution of the current between the phases a, b, and c will depend on the rotor field angle.

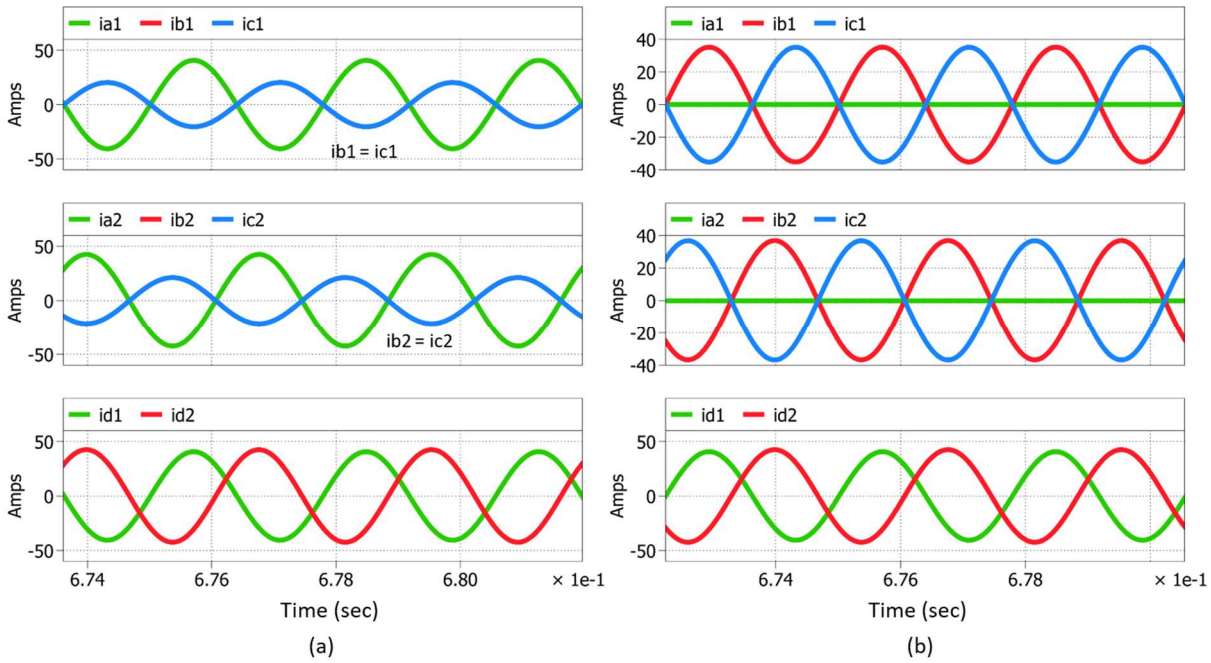

Fig. 3: Stator winding set1 and set2: abc & d-axes currents at rotor electrical angle: (a) 0° (b) 90°

Power flow model

Fig. 4. shows the equivalent T-model of the two d-axes of the synchronous machine during the charging process. In this image, Z_{ds1} represents the impedance of the series connection of l_{ls1} and r_{s1}, (Fig. 2c), Z_{ds2} is the impedance of the series connection of l_{ls2} and r_{s2}, while Z_{eq} is the parallel combination of d-axis magnetizing inductance l_{md} and field winding impedance (series connection of l'_{fr} , r'_{fr}). V_{ds1} and V_{ds2} represent the d-axes rms voltages of winding set1 and set2, whereas I_{ds1} and I_{ds2} represent the d-axes rms currents of the winding set1 and set2.

Please note, that unlike traditional *dq* frame models the quantities $\boldsymbol{I_{ds1}}$ and $\boldsymbol{I_{ds2}}$ are AC phasors and are given by (10) and (11). As such, they have a real part $I_{ds1,x}$ (defined as being in-phase with the winding set2 voltage phasor $\boldsymbol{V_{ds2}}$), along with an imaginary part $I_{ds1,y}$ (defined as being orthogonal to $\boldsymbol{V_{ds2}}$). The real part $I_{ds1,x}$ can be used to transfer real power from winding set1 to set2. Similarly, $I_{ds1,y}$ can be used to supply reactive power. $\boldsymbol{I_{eq}}$ and $\boldsymbol{V_{eq}}$ are the current through and the voltage across the impedance Z_{eq}.

P_1 and P_2 depict the power of the three-phase windings on the DC-grid and battery sides respectively, given by (13) and (14). Ideally, V_{ds1} and V_{ds2} voltages should be near to the rated winding voltage, for higher power flow to be achieved, provided the current $\boldsymbol{I_{eq}}$ does not become excessive. This suggests a high value of Z_{eq} is beneficial for power transfer, limiting reactive currents and system efficiency.

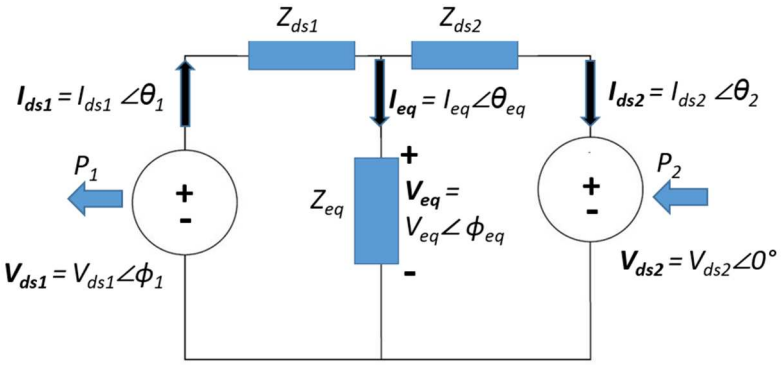

Fig. 4: Equivalent T-model of synchronous machine d-axes during the charging operation

$$\boldsymbol{I_{ds1}} = I_{ds1,x} + jI_{ds1,y} \tag{10}$$

$$\boldsymbol{I_{ds2}} = I_{ds2,x} + jI_{ds2,y} \tag{11}$$

$$\boldsymbol{I_{eq}} = \boldsymbol{I_{ds1}} - \boldsymbol{I_{ds2}} \tag{12}$$

$$P_1 = Re\{\boldsymbol{V_{ds1}} \boldsymbol{I^*_{ds1}}\} \tag{13}$$

$$P_2 = Re\{\boldsymbol{V_{ds2}} \boldsymbol{I^*_{ds2}}\} \tag{14}$$

Controllers

Fig. 5 shows the control schematic for DC charging. Two PR controllers, one for i_{ds1} and another i_{qs1} are deployed. The i_{ds1} PR controller regulates real and reactive power exchange between the two sets of windings. The i_{qs1} PR controller ensures zero AC current flowing in the q-axis. Winding set2 voltages are directly assigned with $v_{ds2*} = \sqrt{2} V_{ds2} cos(\omega t)$, which is consistent with Fig. 4, and $v_{qs2*} = 0$.

A PI controller generates the required real part $I_{ds1,x}$ (of phasor current $\boldsymbol{I_{ds1}}$) needed for dc power transfer, P_{ref}. The imaginary part $I_{ds1,y}$ can be chosen to provide approximately half of the magnetizing branch reactive current. Based on the two components of the required phasor current $\boldsymbol{I_{ds1}}$, the time domain current reference $i_{ds1,ref}$ is fabricated. The modulating signals are generated by normalizing v_{abc1*} and v_{abc2*} to v_{dc1} and v_{dc2} respectively. The rotor angular position θ is taken from an encoder and is used for all rotating reference frame conversions.

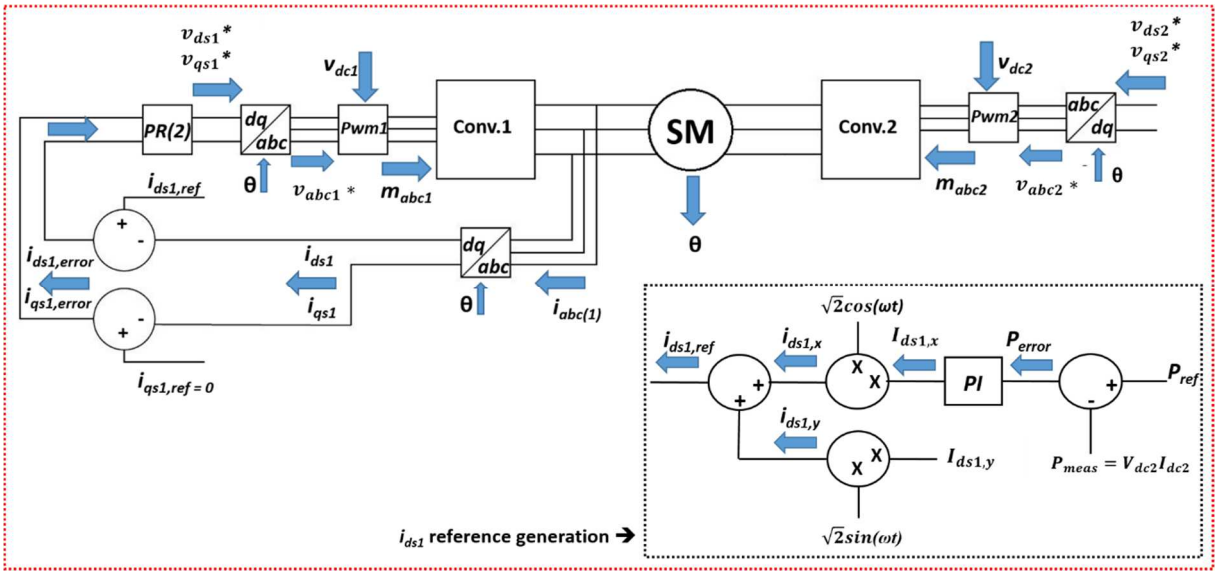

Fig. 5: DC charger control scheme for power transfer while ensuring zero torque production+

Results

The following subsections show the simulated and experimental results using the WFSM and then simulated results using an equivalent PMSM model are shown, emphasizing the higher power transfer using PMSM.

Simulation results

The proposed charger topology has been simulated using the six-phase WFSM machine. The machine used has ratings of 110V rms (line-line), and 40A rms per phase. The DC-link voltage on both inverters (battery and DC grid voltages) is set to 200V, with an inverter switching frequency of 10 kHz. The frequency of the d-axis reference current was set to 360 Hz.

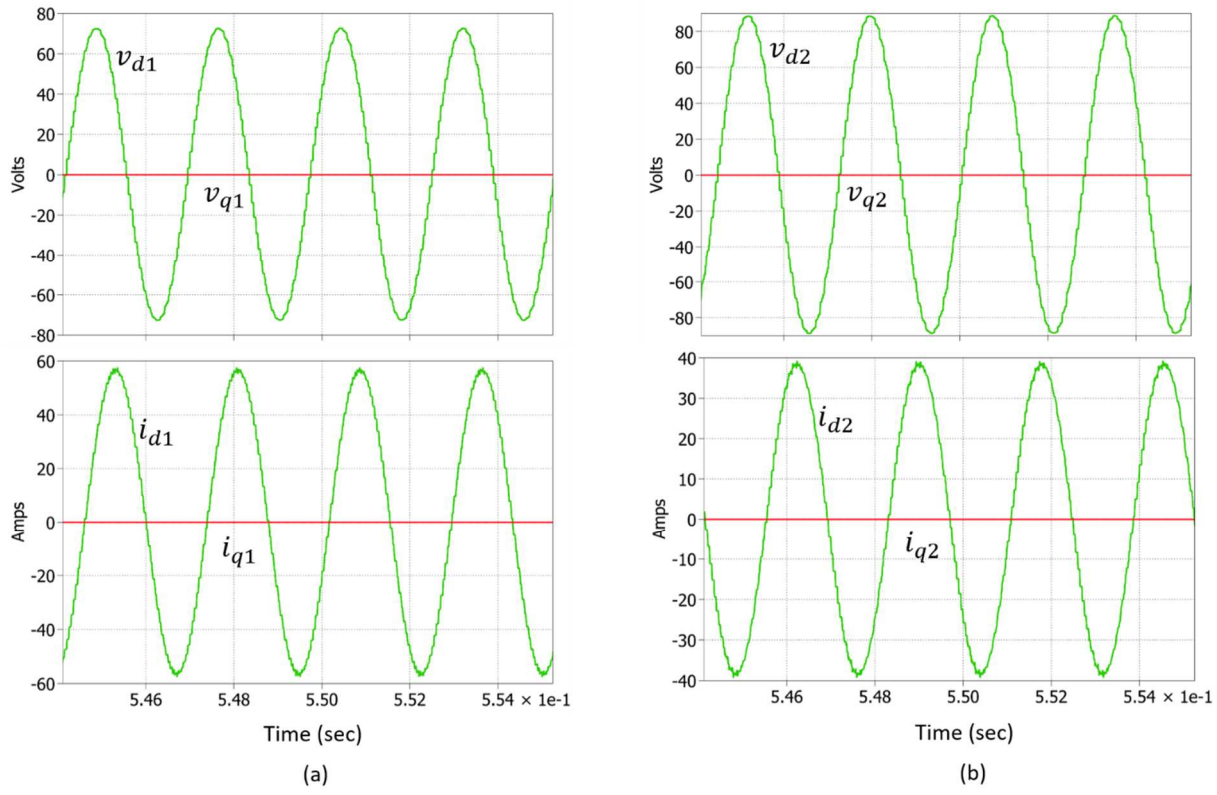

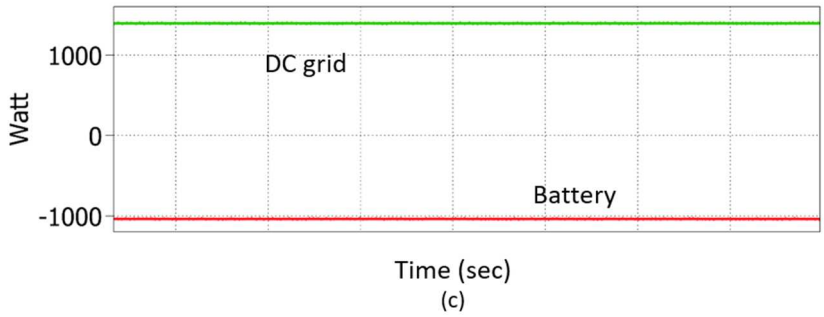

Fig. 6: dq-axes voltages and currents: (a)winding set1 (b)winding set2 (c) DC grid and battery power

Fig 6(a) and Fig 6(b) show the dq-axes voltages and currents of winding set1 and set2 respectively, at a rotor electrical angle of 0°. The q-axis voltages are not excited, therefore, the q-axis currents i_{q1} & i_{q2} remains zero. Hence, the electromagnetic torque is zero. Fig. 6(c) shows the DC power transferred from the DC grid to the battery. Power sent and received is 1394W and 1039W respectively.

Experimental results

The proposed charger topology has been experimentally validated using a six-phase WFSM with parameters shown in Table I. Fig. 7(a) shows the phase voltage and three-phase currents in both the winding sets in the abc frame at 0° rotor electrical angle. Fig. 7(b) shows the corresponding d and q axes currents. Currents i_{q1} & i_{q2} remains zero, indicating that the torque production is zero, based on the torque equation (9).

Table I: Six-phase WFSM parameters

Stator winding resistance ($r_{s1} = r_{s2}$, Fig. 2)	50.5 mΩ
Stator winding leakage inductance ($l_{ls1} = l_{ls2}$, Fig. 2)	0.2788 mH
Stator d-axis magnetizing inductance (l_{md}, Fig. 2)	1.1381 mH
Rotor resistance referred to winding set1 (r'_{fr}, Fig. 2)	65.3 mΩ
Rotor leakage inductance referred to winding set1 (l'_{fr}, Fig. 2)	0.3314 mH
Equivalent branch Impedance (Z_{eq} at 360 Hz, Fig. 4)	(0.04245 + j0.605253)Ω

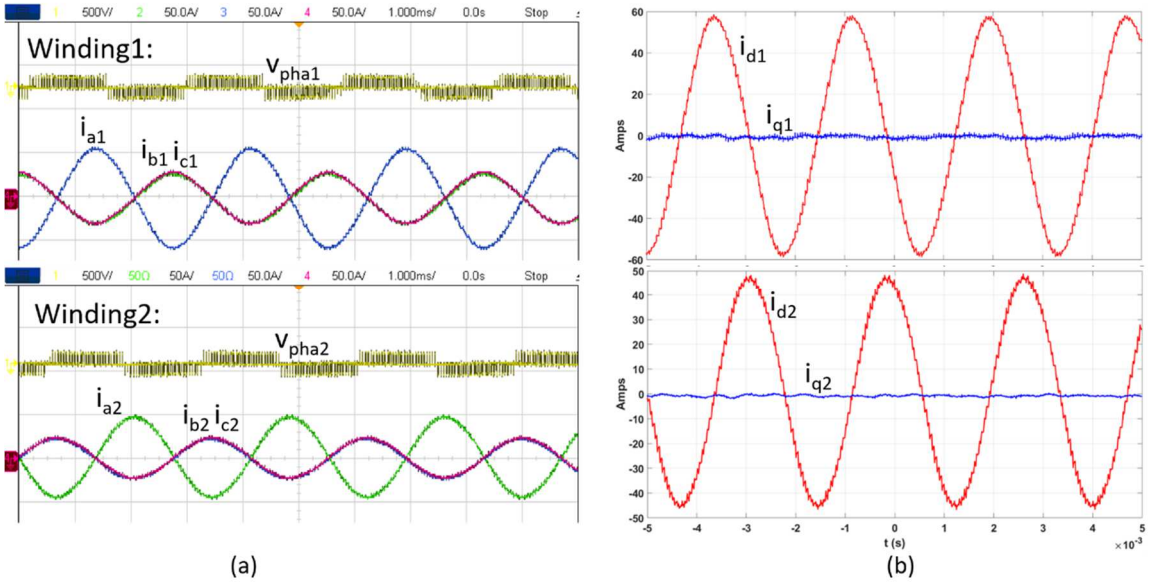

Figure 7. Winding set1and set2: (a) Phase voltage & abc currents (b) dq axes currents.

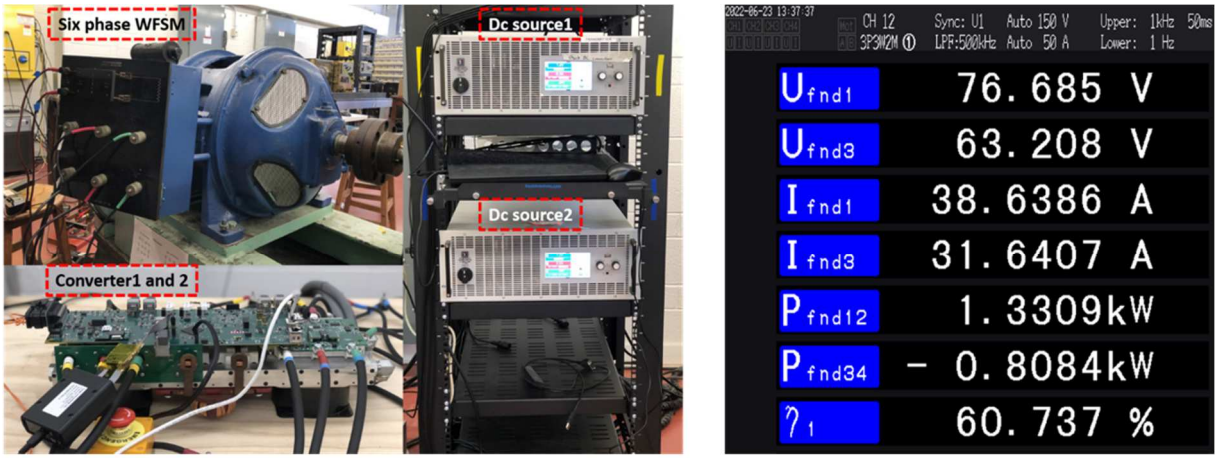

(a) (b)

Fig 8: (a) Experimental setup (six-phase WFSM, dual inverter system, and two DC sources) (b) power analyzer results: machine line voltages, currents, power, and efficiency.

Fig. 8(a) shows the experimental setup used to validate the topology while Fig. 8(b) shows the power analyzer results for the power transfer during the charging operation, where line-line voltages and line currents on each winding set are shown. Power sent and received is 1330.9W and 808.4W respectively from each winding set. The lower efficiency is due to lower equivalent impedance Z_{eq} (in Fig. 4.) resulting in a higher magnitude of equivalent magnetizing branch current ***Ieq***. The additional losses can be attributed to the machine winding ac resistance and core losses.

Simulation Results: PMSM Equivalent Model

The proposed charger topology can be implemented using a PMSM to increase the power transfer capability and particularly efficiency. The short-circuited field winding in the case of WFSM was needed to avoid a large induced voltage on the field but it results in a lower equivalent impedance Z_{eq} (in Fig. 4.). It is also associated with the rotor current conduction and I^2R losses in the rotor circuit. Compared to WFSM, PMSM has no rotor field winding, which needs to be short-circuited, and accordingly will have a higher Z_{eq}. Tables I and II include the value of Z_{eq} for WFSM and PMSM respectively. As a result of higher Z_{eq}, higher power transfer is possible, and a higher efficiency since a smaller magnitude of equivalent magnetizing branch current ***Ieq*** will be produced for a given ***Veq*** (in fig. 4.). Equivalent six-phase PMSM parameters are shown in Table II

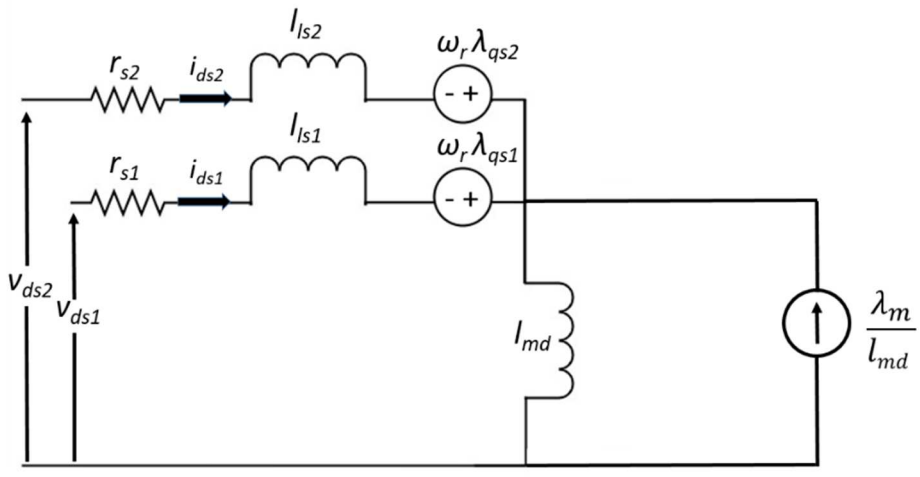

Fig 9: Six-phase PMSM d-axes equivalent circuit, permanent magnet flux linkage is modelled as a current source.

Fig. 9 shows the d-axis equivalent model for a six-phase PMSM, where the permanent magnet flux linkage is modelled as a DC source, and λ_m is the flux linkage due to permanent magnets. The machine stator voltage equations in the d-axis can be given by (15), (16), where λ is flux linkage, ω_r is the rotor speed in electrical radians per second (which is zero during charging), and p is the time derivative. The stator flux linkage equations in d-axis are given in (17), (18) where l_{ls1} and l_{ls2} are the stator leakage inductances, l_{md} is the d-axis magnetizing inductance. The q-axis model will not be discussed here and at zero rotor speed, rotor magnetic flux will not affect the q-axis operation. Fig 10(a) and Fig 10(b) show the dq-axes voltages and currents of winding set1 and set2 respectively, at a rotor electrical angle of 0°. The q-axis currents i_{q1} & i_{q2} are equal to zero. Hence, the electromagnetic torque is zero. Fig. 10(c) shows the DC power transferred from the DC grid to the battery. Power sent and received is 2106W and 2000W respectively. This corresponds to maximum theoretical efficiency of about 95%, compared to the WFSM simulation of Fig 6 where theoretical efficiency is approximately 75%.

$$v_{ds1} = r_{s1} i_{ds1} + p\lambda_{ds1} - \omega_r \lambda_{qs1} \tag{15}$$

$$v_{ds2} = r_{s1} i_{ds2} + p\lambda_{ds2} - \omega_r \lambda_{qs2} \tag{16}$$

$$\lambda_{ds1} = l_{ls1} i_{ds1} + l_{md}(i_{ds1} + i_{ds2}) + \lambda_m \tag{17}$$

$$\lambda_{ds2} = l_{ls2} i_{ds2} + l_{md}(i_{ds1} + i_{ds2}) + \lambda_m \tag{18}$$

Table II:Equivalent Six-phase PMSM parameters

Stator winding resistance ($r_{s1} = r_{s2}$, Fig. 2)	50.5 mΩ
Stator winding leakage inductance ($l_{ls1} = l_{ls2}$, Fig. 2)	0.2788 mH
Stator d-axis magnetizing inductance (l_{md}, Fig. 2)	1.1381 mH
Equivalent branch Impedance (Z_{eq} at 360 Hz, Fig. 4)	j3.1237 Ω

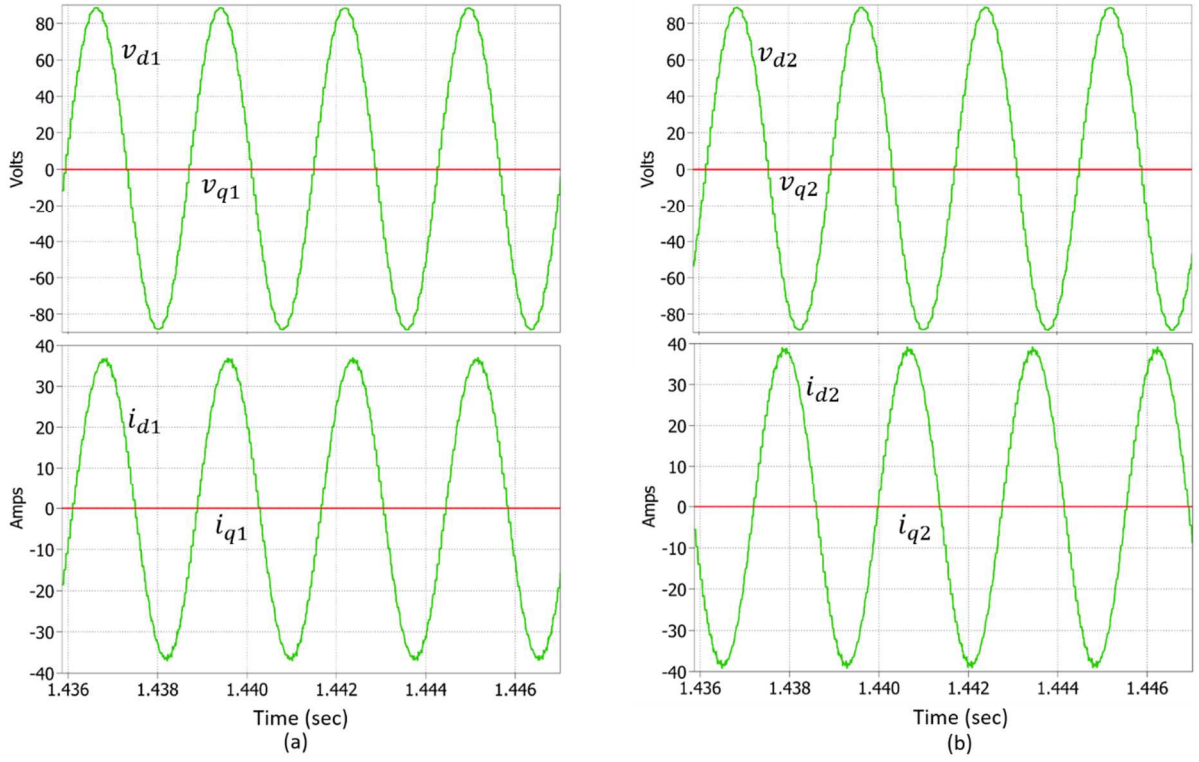

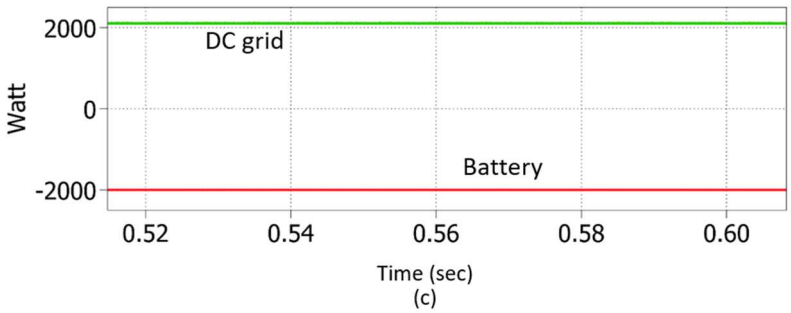

Fig. 10: dq-axes voltages and currents: (a)winding set1 (b)winding set2 (c) DC grid and battery power

Conclusions

This paper presented an isolated integrated DC charger topology based on a six-phase synchronous machine, which requires a minimum reconfiguration from driving and charging modes. The proposed control scheme produces zero average torque and allows power transfer magnetically between two isolated winding sets by injecting a time-varying d-axis current into the stator windings of the machine. The algorithm was experimentally validated with a six-phase wound field synchronous machine and was shown to allow isolated power transfer with zero torque production. The power transfer capability and efficiency of the proposed charger can be greatly increased by using a permanent magnet synchronous machine.

References

[1] A. Salem and M. Narimani, "A Review on Multiphase Drives for Automotive Traction Applications," in *IEEE Transactions on Transportation Electrification*, vol. 5, no. 4, pp. 1329-1348, Dec. 2019

[2] I. Subotic, N. Bodo, E. Levi, B. Dumnic, D. Milicevic and V. Katic, "Overview of fast on-board integrated battery chargers for electric vehicles based on multiphase machines and power electronics", *IET Electric Power Applications*, vol. 10, no. 3, pp. 217-229, March 2016

[3] Bojoi, A. Tenconi, F. Profumo and F. Farina, "Dual-Source Fed Multi-phase Induction Motor Drive for Fuel Cell Vehicles: Topology and Control," *2005 IEEE 36th Power Electronics Specialists Conference*, 2005

[4] M. Y. Metwly, M. S. Abdel-Majeed, A. S. Abdel-Khalik, R. A. Hamdy, M. S. Hamad and S. Ahmed, "A Review of Integrated On-Board EV Battery Chargers: Advanced Topologies, Recent Developments and Optimal Selection of FSCW Slot/Pole Combination," in *IEEE Access*, vol. 8, pp. 85216-85242, 2020

[5] C. Viana, S. Semsar, M. Pathmanathan and P. W. Lehn, "Integrated Transformerless EV Charger With Symmetrical Modulation," in *IEEE Transactions on Industrial Electronics*, vol. 69, no. 12, pp. 12506-12516, Dec. 2022

[6] F. Lacressonniere and B. Cassoret, "Converter used as a battery charger and a motor speed controller in an industrial truck," *2005 European Conference on Power Electronics and Applications*, 2005, pp. 7 pp.-P.7

[7] S. Haghbin, K. Khan, S. Zhao, M. Alakula, S. Lundmark and O. Carlson, "An Integrated 20-kW Motor Drive and Isolated Battery Charger for Plug-In Vehicles," in *IEEE Transactions on Power Electronics*, vol. 28, no. 8, pp. 4013-4029, Aug. 2013

[8] E. Hoevenaars, T. Illg and M. Hiller, "Novel Integrated Charger Concept Using an Induction Machine as Transformer at Standstill," *2020 IEEE Vehicle Power and Propulsion Conference (VPPC)*, 2020, pp. 1-5

[9] P. Pescetto and G. Pellegrino, "Isolated Semi Integrated On-board Charger for EVs Equipped with 6-phase Traction Drives," *IECON 2021 – 47th Annual Conference of the IEEE Industrial Electronics Society*, 2021, pp. 1-6

[10] K. T. Chau, C. C. Chan and C. Liu, "Overview of Permanent-Magnet Brushless Drives for Electric and Hybrid Electric Vehicles," in *IEEE Transactions on Industrial Electronics*, vol. 55, no. 6, pp. 2246-2257, June 2008

[11] R. F. Schiferl and C. M. Ong, "Six Phase Synchronous Machine with AC and DC Stator Connections, Part I: Equivalent Circuit Representation and Steady-State Analysis," in *IEEE Transactions on Power Apparatus and Systems*, vol. PAS-102, no. 8, pp. 2685-2693, Aug. 1983

[12] P. C. Krause, O. Wasynczuk, and S. D. Sudhoff,Analysis of ElectricMachinery and Drive Systems, 2nd ed. Piscataway, NJ, USA: IEEE Press,2002